scientific reports

Check for updates

OPEN

Rate-distortion trade-off analysis of the power-domain ISAC waveform for the unmanned aerial vehicle

Gen Li[1], Lei Xiao[1], Junyi Du[1], Yanbo Sun[1], Dadong Ni[1], Yuansheng Wu[1], Jiale Wang[2], Yifan Guo[2], Jie Lian[2]✉ & Peng Wu[3]✉

Integrated sensing and communication (ISAC) systems greatly promote the development of radio communication and sensing in the sixth-generation era. Meanwhile, the unmanned aerial vehicle (UAV) provides larger coverage and efficiency for multiple user communication and sensing due to the high mobility. Thus, the merging of these two techniques is promising for future wireless communication. However, the main problem is how to design a proper transmitting waveform that is suitable for high-mobility UAV communication while offering good sensing ability. In this paper, we propose the combination of the orthogonal time-frequency-space modulation (OTFS) and the frequency-modulated continuous wave (FMCW) using the power-domain superposition to achieve the high-mobility communication and sensing function. The OTFS modulation is used to resolve the Doppler shift of the communication and FMCW waveform guarantees the sensing ability. We also discuss the ratio-distortion trade-off between sensing and communication function. The numerical results validate the effectiveness of the proposed waveform.

Keywords ISAC, UAV, OTFS, Power-domain, Rate, Distortion

Integrated sensing and communication (ISAC) systems embody a new trend in wireless technology, which brings the opportunity for wireless communication, such as wireless imaging[1,2]. These systems combine communication and sensing capabilities in a unified hardware framework to enhance resource utilization and cost-effectiveness[3–5]. Waveform design plays a crucial role in ISAC systems by creating waveforms that can efficiently support both sensing and communication functions at the same time[6–9].

Based on the fundamental purpose of ISAC systems, the design techniques of ISAC waveforms are commonly grouped into communication-centric, sensing-centric, and joint waveforms. Furthermore, ISAC waveforms can be further classified as communication-based waveforms [10–13] and superposition waveforms[14–18], according to structure of the waveforms. Communication-based ISAC waveforms represent that ISAC systems use standard communication signals, such as OFDM signals, or precoded communication signals as the transmitted signal to achieve the communication and sensing functions simultaneously. For standard communication waveforms, the ISAC systems generally do not pay additional attention to the communication function, however, it requires sophisticated estimation algorithms employed at the sensing receiver to extract target parameters from the communication echoes[10,11]. Although various parameter estimation algorithms are explored, the inherent randomness of communication signals still leads to terrible sensing performance[19], failing to achieve the trade-off performance between communication and sensing of the ISAC systems. In order to achieve the trade-off performance, the researchers use precoding techniques to enhance the sensing ability of standard communication signals. They generally achieved a precoded ISAC waveform design by incorporating the beamforming matrix designs into the ISAC precoder, where the beamforming matrix is optimized considering the communication and sensing performance constraints simultaneously[12,13,20,21].

Superposition waveforms combine random communication and specific sensing signals to form ISAC signals. They offer distinct advantages over communication-based waveforms. Notably, each ISAC symbol contains a deterministic sensing signal, ensuring reliable sensing performance per symbol rather than from a statistical

[1]Southwest China Institute of Electronic Technology, Chengdu 610036, Sichuan, China. [2]School of Marine Science and Technology, Northwestern Polytechnical University, Xi'an 710072, Shaanxi, China. [3]Xi'an Modern Control Technology Research Institute, Xi'an 710072, Shaanxi, China. ✉email: jielian@nwpu.edu.cn; wupengrock@163.com

viewpoint as seen in communication-based waveforms. Moreover, in ISAC systems that merge MIMO radar and multi-user communication, superposition waveforms allow the sensing function to maximize the virtual aperture[22]. Nevertheless, managing interference in superposition-waveform ISAC systems poses challenges. In an effort to enhance resource efficiency, some researchers explore the integration of sensing and communication within the same resource block, referred to as full-superposition waveforms. However, using this waveform makes it notably challenging to effectively mitigate sensing interference for communication signals. In[14], authors propose a sensing interference-removing scheme inspired by NOMA and successive interference canceling (SIC) for full-superposition waveforms. The approach involves treating a portion of the sensing signals as virtual communication symbols and employing SIC to eliminate them, thereby reducing interference for actual communication symbols. However, the study overlooks the residual noise that remains post-removal of virtual communication symbols, which constitutes a portion of the sensing interference, in their theoretical framework. Moreover, in[23], the authors incorporate part of the communication information into sensing signals, allowing users to enhance communication capacity through demodulation. Yet, they still fail to account for residual noise from the sensing signal post-SIC. So the communication performance is not satisfied. In order to reduce further the mutual-interference of sensing and communication signals, the authors introduced a quantization-based full-superposition waveform that presents a fresh approach for ISAC waveforms[15], which involves quantizing the sensing signal solely at the ISAC transmitter. This technique has the potential to efficiently remove sensing interference at the communication receivers through a simpler operation compared to current methods.

The ISAC technique offers additional methods for communicating and monitoring specific objectives. Incorporating unmanned aerial vehicles (UAVs) into ISAC networks can significantly enhance their effectiveness. UAVs, being cost-effective aerial platforms, can improve ISAC services by providing broader coverage and a more reliable Line-of-Sight (LoS) connection. By capitalizing on UAVs' mobility and strong air-to-ground LoS channels, UAV-enabled ISAC systems can deliver superior sensing and communication performance. However, this innovative approach presents unique design challenges, particularly related to the stringent size, weight, and power constraints imposed on UAVs, which can limit their communication and sensing capabilities. Therefore, formulating strategies for designing UAV-enabled ISAC systems to optimize sensing and communication performance while ensuring effective coordination among UAVs is a novel and intricate issue to tackle. Given the points above, there is a need to investigate a unified ISAC waveform for UAV-enabled systems to enhance spectrum efficiency. The superposition waveform emerges as a viable choice as it permits the reuse of power-domain resources, unencumbered by antenna aperture constraints, thereby reducing the size and payload requirements of UAVs.

In this paper, we propose using the combination of orthogonal time-frequency-space modulation (OTFS) and power-domain superposition waveform to provide a robust communication sensing performance, as shown in Fig. 1. OTFS modulation maps information symbols into the delay–Doppler (DD) domain, allowing them to effectively capture time and frequency variations in high-mobility channels, which is crucial for UAV communication. Meanwhile, FMCW signals are classical radar waveforms that ensure high-precision range and velocity estimation, making them ideal for sensing tasks. Motivated by these properties, this paper combines OTFS and FMCW through a power-domain superposition scheme to achieve robust communication and sensing simultaneously. The power-domain superposition ISAC waveform is designed in the DD domain to provide sensing and communication abilities at the same time-frequency-space resource. Then, the ISAC waveform is modulated by OTFS in order to fit in the high-mobility communication channel due to the UAV flying. We also discuss the optimal power-domain ISAC waveform in terms of the rate-distortion trade-off viewpoint, where the power allocation index and quantization order are optimized according to the sensing and

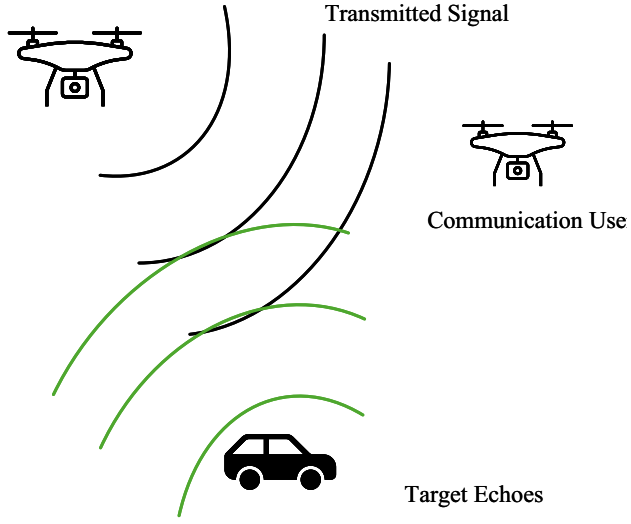

Fig. 1. Illustration of the UAV-ISAC systems.

communication requirements. The simulation results demonstrate the effectiveness of the proposed waveform for UAV communication and sensing.

Transmitted signal model

In this paper, we consider a UAV with sensing and communication functions using the same time-frequency resources. For UAVs, they generally are controlled to form a special swarm for some specific tasks, so they need to communicate and sense with each other to keep the formation. Now, we first introduce the transmitted ISAC signal and received signals at the communication end and sensing end model, respectively. Notably, we consider the mono-static ISAC system in this work where the sensing receiver and ISAC transmitter are colocated.

Power-domain ISAC waveform

Due to the high mobility property of the UAV, the Doppler frequency shift is severe, degrading the performance of conventional communication schemes, such as orthogonal frequency division multiplexing (OFDM). In order to remove the Doppler frequency shift easily, the OTFS modulation is used.

At first, we generate a binary sequence. Then, the binary sequence is mapped into a symbol using a *Q*-QAM constellation. After that, the symbols are formed as an $M \times N$ matrix X_c

$$\mathrm{X}_c = \begin{bmatrix} x^c_{0,0} & x^c_{0,1} & \cdots & x^c_{0,M-1} \\ x^c_{1,0} & x^c_{1,1} & \cdots & x^c_{1,M-1} \\ \vdots & \vdots & \cdots & \vdots \\ x^c_{N-1,0} & x^c_{N-1,1} & \cdots & x^c_{N-1,M-1} \end{bmatrix}, \tag{1}$$

where *M* and *N* denote the numbers of delay bins and Doppler bins in the DD domain, respectively. The matrix X_c represents the conveyed communication information in the Delay-Doppler domain. Then, we introduce the design of the sensing signal in the DD domain, and the two signals are combined to generate the power-domain ISAC signal.

As stated in Ref.[15], the power-domain ISAC waveform design relies on the quantization of the sensing signal. Thus, we generate the sensing radar signal. To align with existing radar systems, we use the classical frequency-modulated continuous wave (FMCW) signal as the original radar signal, which is generated by

$$\begin{aligned} f(t) &= \sum_{m=0}^{M-1} e^{j2\pi(f_0 t + \kappa t^2)} G_{\mathrm{RC}}(t - mT) \\ &= \sum_{m=0}^{M-1} e^{j2\pi(f_0 t + B/T t^2)} G_{\mathrm{RC}}(t - mT), \end{aligned} \tag{2}$$

where *j* is the imaginary unit, f_0 is the carrier frequency, and *M* is the number of the linear frequency-modulated (LFM) signal. $\kappa = B/T$ is the frequency slope, where *B* is the bandwidth of the FMCW signal, *T* is the duration of the LFM signal, and

$$G_{\mathrm{RC}}(t) = \begin{cases} \dfrac{1}{T}\left[1 + \cos\left(\dfrac{\pi t}{\beta T}\right)\right], & |t| \le \dfrac{\beta T}{2}, \\ \dfrac{1}{T}, & \dfrac{\beta T}{2} < |t| \le \dfrac{T}{2}, \\ 0, & \text{otherwise}, \end{cases} \tag{3}$$

is a time-limited function, where $\beta \in [0, 1]$ denotes the roll-off factor that controls the smoothness of the pulse edges. The use of $G_{\mathrm{RC}}(t)$ provides a smooth transition region, which reduces spectral sidelobes and inter-symbol interference. Notably, we need to generate the power-domain ISAC signal in the baseband, so the FMCW signal used here is also generated in the baseband.

Due to the use of the OTFS modulation, we should process the signal in the DD domain. Therefore, the original radar signal should also be converted into the DD domain for further processing. Now, we sample the *m*-th LFM of the FMCW signal in (2) with a sampling rate *B* as

$$s_m(n) = e^{j2\pi\kappa n/B^2}, n = 0, \cdots, N-1, \tag{4}$$

where $\boldsymbol{s}$ is the $N \times 1$ vector, representing the discrete version of the LFM signal. Then, the FMCW signal could be denoted as

$$f(n) = \sum_{m=0}^{M} s_m(n - m(N-1)). \tag{5}$$

Then the delay-time domain signal *f*(*n*) is transformed to the time-frequency domain using the Wigner transform to obtain . The symplectic fast Fourier Transform (SFFT) is applied to the time-frequency domain matrix to obtain the delay-Doppler domain form

$$F_{n,m} = \frac{1}{\sqrt{MN}} \sum_{k=0}^{N-1} \sum_{l=0}^{M-1} \mathrm{f}[l,k] e^{-j2\pi(\frac{nk}{N} - \frac{ml}{M})}, \tag{6}$$

where $\mathrm{f}[l,k]$ is the *l*th row, *k*th column element of . Then the $F_{n,m}$ could also form a matrix as

$$\mathrm{F} = \begin{bmatrix} F_{0,0} & F_{0,1} & \cdots & F_{0,M-1} \\ F_{1,0} & F_{1,1} & \cdots & F_{1,M-1} \\ \vdots & \vdots & \cdots & \vdots \\ F_{N-1,0} & F_{N-1,1} & \cdots & F_{N-1,M-1} \end{bmatrix}. \tag{7}$$

Notably, because of the property of the DD domain for this periodic signal *f*(*t*), the elements of the matrix F satisfy

$$F_{n,m}|_{n\neq 0} = 0. \tag{8}$$

In other words, the element of the first column of F is non-zero, but the other elements must be zero. This property will help in signal separation at the communication user, providing an advantage, as we will show in the next section.

Then, we should quantize the sensing signal matrix F to enable the power-domain ISAC waveform as

$$\mathrm{X}^s = Q(\mathrm{F}, L_s). \tag{9}$$

The operator $Q(\cdot, L_s)$ represents a uniform real-valued quantization function with quantization order L_s , applied to the sensing signal matrix F to obtain the quantized sensing waveform X^s. In this paper, the quantizer has the following requirements: (1) The order L_s should be odd due to some elements of F being zero; (2) the uniform quantizer is considered for simplicity; (3) The real-valued quantizer is used because the F is real-valued. For the general sensing signal, the complex-valued quantization could be considered. According to these requirements, the constellation of quantized sensing signals could be written as

$$X^s_{n,m} \in \left\{-X^{+s}, X^{+s}\right\}, \tag{10}$$

where

$$X^{+s} \in \left\{ \max\{|\mathrm{F}|\},\ \cdots,\ \max\{|\mathrm{F}|\} - l\frac{2\max\{|\mathrm{F}|\}}{L_s - 1},\ \cdots,\ 0 \right\}. \tag{11}$$

After obtaining the communication and sensing signals, we utilize the two signals to generate the ISAC waveform in DD domain. The power-domain ISAC waveform is

$$\mathrm{X} = \sqrt{P_s}\mathrm{X}^s/\sigma_s^2 + \sqrt{P_c}\mathrm{X}^c/\sigma_c^2, \tag{12}$$

where σ_s^2 and σ_c^2 are the power of signal X^s and X^c, respectively. P_s and P_c are the allocated power for sensing and communication signals, with $P_s + P_c = P_t$, where P_t is the total transmitting power. Additionally, $P_s \geq P_c$ because the radar signal generally involves round-trip propagation in the studied monostatic scenario, and the radar cross-section (RCS) of the target is considered weak. Under this scenario, $P_s \geq P_c$ is reasonable.

Then the DD domain ISAC signal is converted into the time-frequency domain to be emitted by using

$$\mathrm{x}[k,l] = \sqrt{MN} \sum_{n=0}^{N-1} \sum_{m=0}^{M-1} X[n,m] e^{j2\pi(\frac{nk}{N} - \frac{ml}{M})}, \tag{13}$$

where $X[n, m]$ is the *n*th row and *m*th column of the matrix X. Finally, we use the Heisenberg transform and add the cyclic prefix (CP) in order to obtain the time-domain transmitting signal $x(t)$. The signal $x(t)$ is then converted and emitted from an antenna on the UAVs.

Received signal model

In this section, we describe the received signal models at the communication user and sensing receiver.

Received communication signal

For the high mobility communication user, the Doppler effect is significant, so the communication channel between transmitter and communication receiver with delay-Doppler representation is

$$h(\tau,\mu)=\sum_{k=1}^{K} g_k\delta(\tau-\tau_k)\delta(\mu-\mu_k), \tag{14}$$

where τ, μ are the delay and Doppler frequency shift, and K is the number of the propagation paths. g_k is the complex channel gain, and δ is the Dirac function. Then the received communication signal passing the channel, after down-convert, could be written as

$$r(t)=\int\int h(\tau,\mu)e^{j2\pi\mu t}x(t-\tau)d\mu d\tau+n_c(t). \tag{15}$$

where $n_c(t)$ is the zero-mean additive Gaussian white noise with variance σ_n^2. When the CP is removed, the signal is converted from serial to parallel, and the Wigner transform and inverse SFFT are executed on it to convert the received signal into the DD domain. The signal in the DD domain is

$$\mathrm{R}=\mathrm{H}*\mathrm{X}+\mathrm{N}_c, \tag{16}$$

where H represents the sampled matrix form of the channel $h(\tau,\mu)$, $*$ denotes the two-dimensional circular convolution operation, and N_c is the DD domain noise of $n_c(t)$. In accordance with Reference [24], the linear minimum mean square error (LMMSE) equalizer is utilized to remove the channel. Define the vectorized forms $\mathrm{r}=\mathrm{vec}(\mathrm{R})$, $\mathrm{x}=\mathrm{vec}(\mathrm{X})$, and $\mathrm{n}_c=\mathrm{vec}(\mathrm{N}_c)$, where $\mathrm{vec}(\cdot)$ is the vectorized operation. Then the system can be written in vector form as

$$\mathrm{r}=C(\mathrm{H})\mathrm{x}+\mathrm{n}_c, \tag{17}$$

where $C(\mathrm{H})\in\mathbb{C}^{NM\times NM}$ is the 2-dimension circular convolution matrix, constructed as

$$C(\mathrm{H})=\sum_{n=0}^{N-1}\sum_{m=0}^{M-1}\mathrm{H}[n,m]\left(\mathrm{P}_N^n*\mathrm{P}_M^m\right), \tag{18}$$

with P_N and P_M being the $N\times N$ and $M\times M$ cyclic permutation matrices. The LMMSE equalizer minimizing $\mathbb{E}\{\|\mathrm{x}-\mathrm{G}_{MMSE}\mathrm{r}\|^2\}$ is

$$\mathrm{G}_{MMSE}=\boldsymbol{\Sigma_x}C(\mathrm{H})^H\left(C(\mathrm{H})\,\boldsymbol{\Sigma_x}C(\mathrm{H})^H+\boldsymbol{\Sigma_n}\right)^{-1}, \tag{19}$$

where $\boldsymbol{\Sigma_x}=\mathbb{E}[\mathrm{x}\mathrm{x}^H]$ and $\boldsymbol{\Sigma_n}=\mathbb{E}[\mathrm{n}_c\mathrm{n}_c^H]$. For independent and identically distributed transmitted symbols and white Gaussian noise, $\boldsymbol{\Sigma_x}=\sigma_x^2\mathrm{I}$, $\boldsymbol{\Sigma_n}=\sigma_n^2\mathrm{I}$, giving the LMMSE equalizer as

$$\mathrm{G}_{MMSE}=\left(C(\mathrm{H})^HC(\mathrm{H})+\tfrac{\sigma_n^2}{\sigma_x^2}\mathrm{I}\right)^{-1}C(\mathrm{H})^H. \tag{20}$$

After equalizing the channel, (16) is processed as

$$\hat{\mathrm{X}}=\sqrt{P_s}\mathrm{X}^s/\sigma_s^2+\sqrt{P_c}\mathrm{X}^c/\sigma_c^2+\mathrm{N}_{c,eq}. \tag{21}$$

For the communication receiver, the vital problem is to extract the communication symbol X^c from $\hat{\mathrm{X}}$. In order to obtain the communication signal, the quantizer is used again as stated in (9). However, the DD domain has a unique property for this operation. Back to (8), the elements of F are zero for the case $n\neq 0$, leading to the elements of X^s also being zero. Thus, we only need to process the first column of $\hat{\mathrm{X}}$, i.e., $\hat{\mathrm{x}}_1$, to obtain the quantized sensing symbol X^s. We denote the first column of X^s as x^s, the first column of X^c as x^c. Notably, the power ratio between x^s and x^c is $(M-1)P_s/P_c$, the gain $M-1$ comes from the zero elements of X^s. Because the $P_s\geq P_c$, the communication symbol x^c could be viewed as a weaker interference for the quantized sensing symbol x^c. Therefore, we could obtain

$$\hat{\mathrm{x}}^s=Q(\hat{\mathrm{x}}_1/\sqrt{P_s},L_s). \tag{22}$$

Then, the estimation of X^s, i.e.,$\hat{\mathrm{X}}^s$, could be obtained by using $\hat{\mathrm{x}}^s$ and zero padding.

Now, the communication symbols could be obtained as

$$\begin{aligned}\hat{\mathrm{X}}^c&=\sigma_c^2\frac{\hat{\mathrm{X}}-\sqrt{P_s}\hat{\mathrm{X}}^s/\sigma_s^2}{\sqrt{P_c}}\\&=\sigma_c^2\frac{\sqrt{P_s}(\mathrm{X}^s-\hat{\mathrm{X}}^s)/\sigma_s^2+\sqrt{P_c}\mathrm{X}^c/\sigma_c^2+\mathrm{N}_{c,eq}}{\sqrt{P_c}}\\&\approx\mathrm{X}^c+\sigma_c^2\frac{\mathrm{N}_{c,eq}}{\sqrt{P_c}},\end{aligned} \tag{23}$$

where the approximation is valid when $P_s \geq P_c$. This approximation is employed solely to illustrate the estimated communication symbols when the sensing symbol is assumed to be perfectly estimated. In the simulation section, we refrain from utilizing this approximation and instead opt for the actual demodulation performance.

From the processing flow, we see that the combination of the FMCW signal and OTFS modulation is more suitable for the power-domain ISAC waveform than OFDM in[15]. The $M-1$ times gain is obtained through the mean operation across multiple OFDM symbols, leading to additional operations and increased complexity. This is also the main advantage of the proposed method.

Rate-distortion trade-off waveform optimization

In the previous section, we introduced the combination of OTFS modulation and FMCW signal for ISAC. However, two vital parameters L_s and $P_s(P_c)$ impact the sensing and communication performance significantly. Some metrics are proposed to evaluate the communication and sensing performance in ISAC systems, such as mutual information[25] and waveform similarity[26]. In this section, we will discuss the optimal parameter selection based on the rate-distortion trade-off for different performance requirements.

Sensing distortion

For the sensing function, the transmitted waveform is important because it determines the lower bound of the sensing performance. However, the performance metrics of the sensing waveform are various, such as Cramér-Rao bound, peak-to-average power ratio, and constant modulus. Therefore, justifying that an ISAC waveform has a better sensing performance is a challenging task.

A reasonable way is to measure the difference between the ISAC waveform and the classical radar waveform, such as the FMCW signal. The classical radar waveforms are generally widely used and have robust sensing performance, so it could be viewed as a reference waveform for sensing function. In this paper, we use the Euclidean distance between the ISAC waveform and the FMCW signal because our ISAC waveform is the combination of communication signal and FMCW. And we named this distance as waveform distortion

$$\begin{aligned} D(L_s, P_s) &= ||\mathrm{X} - \frac{\sqrt{P_t}}{\sigma_s^2}\mathrm{F}||_2^2 \\ &= ||\sqrt{P_s}\mathrm{X}^s/\sigma_s^2 + \sqrt{P_c}\mathrm{X}^c/\sigma_c^2 - \sqrt{P_t}\mathrm{F}/\sigma_s^2||_2^2 \\ &= ||\sqrt{P_s}Q(\mathrm{F}, L_s)/\sigma_s^2 + \sqrt{P_t - P_s}\mathrm{X}^c/\sigma_c^2 - \sqrt{P_t}\mathrm{F}/\sigma_s^2||_2^2. \end{aligned} \tag{24}$$

From (24), we see that the distortion of the sensing signal is impacted by the parameters L_s and P_s. Meanwhile, when P_s approaches P_t, the second term of the third line in (24) is nearly zero. The distortion is only related to the quantization order, and the lower the quantization order, the higher the distortion. When the quantization order L_s approaches infinity, i.e., without quantization, the distortion $D(L_s, P_s)$ becomes zero. In other words, the sensing performance of the ISAC waveform and FMCW signal is the same. Thus, we desire the distortion $D(L_s, P_s)$ to be as low as possible for better sensing performance in the ISAC systems.

Communication rate

For the communication systems, the communication achievable rate is an important metric, which represents the ability of the conveying information to the communication systems. In the proposed system, we could obtain the estimation of X^c using (23), thus the communication capacity, i.e., maximum rate, is

$$\begin{aligned} C_1(P_s, L_s) &= B\log_2\left(1 + \frac{\sigma_c^2}{P_s/P_c||\mathrm{X}^s - \hat{\mathrm{X}}^s||_2^2\sigma_c^2/\sigma_s^2 + \sigma_c^2\sigma_n^2/P_c}\right) \\ &\approx B\log_2\left(1 + \frac{1}{\sigma_n^2/P_c}\right), \end{aligned} \tag{25}$$

where the approximation also is based on the perfect demodulation of the quantized sensing symbol, as shown in (22). However, this capacity has two limitations for the proposed system. First, (25) is valid if the input X^c is subject to a Gaussian distribution, but the real communication symbols X^c in our paper are extracted from an alphabet, leading to the ineffectiveness of this equation. Second, this approximation is ideal when we analyze the impact of the parameters on the performance of this ISAC system, which is held when the P_s is larger than P_c. According to these approximations, we could not see the whole trade-off property in terms of the adjustable parameters. We need to derive the more proper form of the capacity for this system.

At first, the communication rate could be calculated as

$$R(P_s, L_s) = I(\mathrm{X}^c) - I(\mathrm{X}^c|\sqrt{P_s}, \mathrm{X}^s - \hat{\mathrm{X}}^s, L_s), \tag{26}$$

where the I denotes the entropy of the information. The capacity under the used system is

$$C(P_s, L_s) = \max_{P_s, L_s} R(P_s, L_s). \tag{27}$$

According to the definition of entropy of the discrete symbols, we have

$$I(\mathrm{X}^c) = -\sum_{i_1}^{U_1} P(x_{i_1}^c)\log_2 P(x_{i_1}^c), \tag{28}$$

and

$$I(\mathrm{X}^c|\sqrt{P_s}, \mathrm{X}^s - \hat{\mathrm{X}}^s, L_s) = -\int P(y)\sum_{i_1}^{U_1}[P(x_{i_1}^c|y)\log_2 P(x_{i_1}^c|y)]\,dy, \tag{29}$$

where

$$y = \sigma_c^2 \frac{\sqrt{P_s}(x_{i_1}^s - \hat{x}_{i_1}^s)/\sigma_s^2 + \sqrt{P_c}x_{i_2}^c/\sigma_c^2 + n_{c,eq}}{\sqrt{P_c}}. \tag{30}$$

Equation (29) shows that the mutual information $I(\mathrm{X}^c|\sqrt{P_s}, \mathrm{X}^s - \hat{\mathrm{X}}^s, L_s)$ is related with the parameters P_s, constellation of transmitted symbols and the noise level. In fact, the quantization order L_s is implicitly contained in the expression due to the term $\mathrm{X}^s - \hat{\mathrm{X}}^s$. The quantization order L_s and power index P_s impact the value of $\mathrm{X}^s - \hat{\mathrm{X}}^s$.

However, Eq. (29) could not be calculated analytically, because the statistical property of the y is complex and unknown to us. Therefore, we need to obtain it using the Monte Carlo simulation. According to Ref.[27], we have

$$R(P_s, L_s) = \log_2 M_c - \frac{1}{M_c}\sum_{x^c \in \mathscr{X}^c} \mathbb{E}[A(y, x^c)|x^c], \tag{31}$$

where M_c is the modulation size of the communication symbols,

$$A(y, x^c) = \log_2 \frac{\sum_{x^c \in \mathscr{X}^c}\sum_{x_1 \in \mathscr{X}_1} e^{-\frac{P_c|y-(x_1+x^c)|^2}{2\sigma_n^2}}}{\sum_{x_1 \in \mathscr{X}_1} e^{-\frac{P_c|y-(x_1+x^c)|^2}{2\sigma_n^2}}} \tag{32}$$

and

$$x_1 = \sigma_c^2/\sigma_s^2\sqrt{P_s}/\sqrt{P_c}(x_{i_1}^s - \hat{x}_{i_1}^s). \tag{33}$$

The variable y is subjected to a random distribution, and it probability density function is

$$p(y|x^c, x_1) = \frac{1}{\sqrt{2\pi\sigma_n^2}} e^{-\frac{|y-(x_1+x^c)|^2}{2\sigma_n^2}}. \tag{34}$$

We could obtain the $R(L_s, P_s)$ by using Monte-Carlo simulation through (31) to (34).

Trade-off waveform

In the previous subsections, we introduced the sensing distortion and communication rate of the proposed power-domain ISAC waveform. Now, we will discuss the influence of the two adjustable parameters P_s and L_s on these two metrics. For the sensing distortion $D(L_s, P_s)$, we see that the larger P_s is, the larger L_s is, and the better (smaller) the sensing distortion is. In contrast, the larger P_s is, the larger L_s is, and the worse the communication rate is. Therefore, the sensing distortion and communication rate conflict in terms of the two adjustable parameters, as described in common ISAC systems. In order to depict the whole trade-off property of the used power-domain waveform, the following problem should be studied:

$$\begin{aligned} &\min_{P_s, P_c, L_s} D(L_s, P_s) \\ s.t.\quad &R(P_s, L_s) \geq R_0 \\ &P_c + P_s = P_t. \end{aligned} \tag{35}$$

We change the value of R_0 to obtain different values of P_s and L_s in order to reveal the trade-off property between sensing distortion and communication rate using the MCS.

Results

In this section, we examine the proposed ISAC waveform aimed for the UAV, focusing on the communication and sensing performance. Finally, we demonstrate the trade-off property in terms of the rate-distortion criterion. We assume that a UAV is communicating with other users and sensing the environment. The simulation parameters are listed in Table 1.

Parameter	Value
Maximum Velocity of UAV	700km/h
N	64
M	16
P_t	1
σ_n^2	0.01
M_c	4
Carrier Frequency	5.8 GHz
Frequency Spacing Δf	12.5 KHz

Table 1. The simulation parameters.

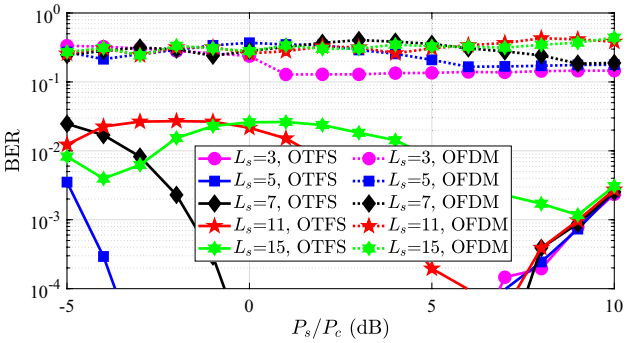

Fig. 2. The BER performance with different power allocation P_s and quantization order L_s using the OTFS and OFDM modulation.

Communication performance

First, we show the communication performance. Considering the line-of-sight (LoS) path of the UAVs, we only assume that the communication user receives the one path with the Doppler shift and delay, and the equalizer is used to remove the channel effect. Notably, the OTFS modulation is used in our paper, so the communication system has the ability to combat the Doppler shift. The communication channel is randomly generated in each simulation, and the results shown here are the statistic property.

As shown in Fig. 2, we first show the bit error rate (BER) performance under different power allocation indices P_s and quantization orders L_s. We see that communication performance is good when the quantization order is smaller, such as $L_s = 3, 5, 7$. When the quantization order becomes higher, the BER is worse. Meanwhile, we note that when P_s is much larger than P_c, the communication performance is worse than the case where P_s is larger than P_c. The reason is the overly small P_c leading to the degradation of communication anti-noise ability. If the total transmitting power P_t is increased, the communication performance will improve. More importantly, we note that when P_s is smaller than P_c, the communication performance with a lower quantization order is still good. Generally speaking, this is considered impossible because the sensing interference cannot be properly removed in this case. However, due to the processing gain of OTFS modulation for FMCW signal, the power of the sensing signal is enhanced, resulting in correct demodulation even when $P_s < P_c$. In addition, we also simulate the case where the UAV adopt the OFDM modulation to generate the power-domain ISAC waveform, and the results are plotted in Fig. 2. Obviously, the communication BER is terrible than the case using OTFS modulation because the frequency shift caused by the high-speed moving can not be handled well. The results highlight the advantage of the OTFS modulation in the high-speed moving scenario.

Moreover, we also show the communication rate in Fig. 3. From Fig. 3, we see that the communication rate is almost $\log_2 M_c$ for a smaller quantizer at any P_s/P_c, which means the communication information is successfully conveyed. Similarly, with the increase of the quantization order L_s, the rates also decrease. The varying rate curves correspond to the BER curves in Fig. 2. The reason for the variation is that the power ratio P_s/P_c does not linearly impact the communication performance. When P_s/P_c increases initially, it means the power of the communication signal is improved, while the power of the sensing signal is much larger than that of the communication signal. Therefore, the communication signal cannot interfere with the sensing signal, leading to the successful demodulation of the sensing symbol. Subsequently, the communication symbols are demodulated without sensing interference, and the performance is enhanced with the communication power. However, when the P_s/P_c increases further, the communication power is basically the same as the sensing power, resulting in the failure of demodulating the sensing signal. The residual sensing signal interferes with the communication signal, degrading the communication performance.

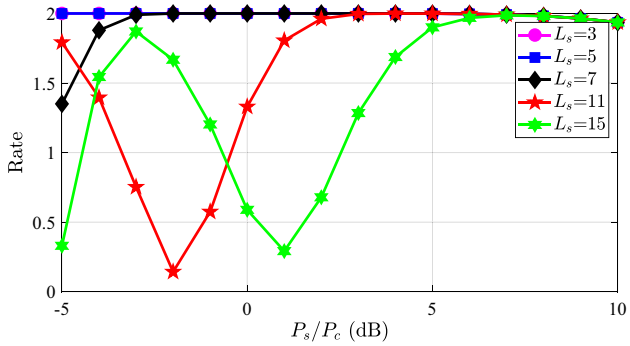

Fig. 3. The communication rate with different power allocation P_s and quantization order L_s using the OTFS modulation.

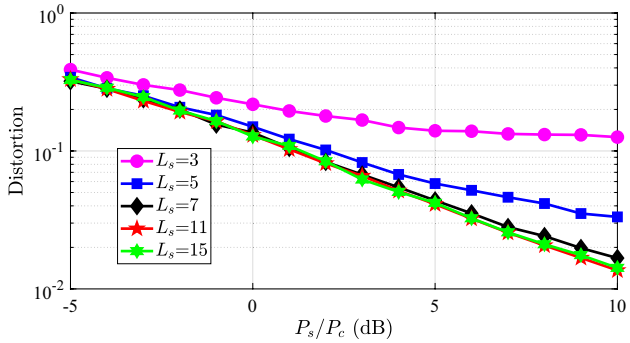

Fig. 4. The sensing distortion with different power allocation P_s and quantization order L_s using the OTFS modulation.

Sensing performance

Then, we discuss the distortion metric of the sensing function in Fig. 4. The variation of the distortion is simple compared with the communication performance. The distortion always decreases as the P_s/P_c and L_s increase. The reason is evident: the slighter the quantization, the more components in the ISAC waveform, and the smaller distortion is obtained. The distortion performance is not impacted by the additive noise. Additionally, we should note that with higher quantization orders, such as $L_s = 7, 11$, and 15, the distortion performances are almost the same. This result means we could choose a lower quantization order to guarantee the communication performance while keeping the distortion almost invariant. An overly high quantization order not only brings little sensing performance gain but also severely degrades the communication performance.

Trade-off performance

For the ISAC systems, the most important thing is that the system should have flexible controllable performance between sensing and communication functions. In order to show the flexibility, we plot the rate-distortion performance of the proposed waveform in Fig. 5. In Fig. 5, we see that the quantization has the obvious influence on the balance between sensing and communication performance. When the quantization order is small, i.e., $L_s = 3$, the sensing distortion is much larger than other cases of quantization order, which means the small quantization order can not achieve a good trade-off performance. With the quantization order increasing, the curves are moving to the left-up corner, where the optimal trade-off performance occurs. Especially, when the quantization order $L_s = 11$, the optimal trade-off is achieved, as shown in the mini-figure in Fig. 5. These results show that the adjustable parameters L_s and P_s could satisfy the requirement of the UAV-ISAC systems.

Conclusions

Integrated sensing and communication systems play a crucial role in advancing radio communication and sensing in the sixth-generation era. Simultaneously, unmanned aerial vehicles enhance communication and sensing capabilities by offering expansive coverage and efficiency, thanks to their high mobility. Combining these technologies holds great promise for the future of wireless communication. However, a key challenge lies in devising a suitable transmitting waveform that caters to high-mobility UAV communication while maintaining robust sensing capabilities. In this study, we advocate for integrating OTFS with FMCW using power-domain superposition to enable efficient high-mobility communication and sensing. OTFS modulation addresses Doppler shifts in communication, while FMCW waveform ensures effective sensing. We also explore the trade-

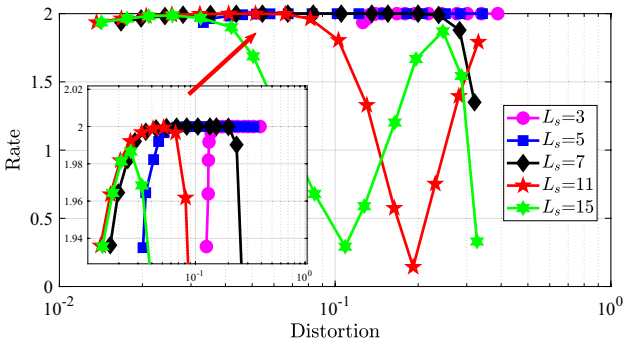

Fig. 5. The rate-distortion trade-off performance of the proposed waveform.

off between sensing and communication functions concerning ratio distortion. Numerical results affirm the efficacy of our proposed waveform design.

The datasets generated during and/or analysed during the current study are available from the corresponding author on reasonable request.

Data availability

The datasets generated during and/or analysed during the current study are available from the corresponding author on reasonable request.

Received: 16 September 2025; Accepted: 13 November 2025
Published online: 22 November 2025

References

1. Bazzi, A., Ying, M., Kanhere, O., Rappaport, T. S. & Chafii, M. Isac imaging by channel state information using ray tracing for next generation 6g. *IEEE J. Sel. Top. Electromagn. Antennas Propag.* **1**(1), 135–149 (2025).
2. Zhang, Y., Zhang, Z., Tong, X. & wen Huang, C. 3d environment sensing with channel state information based on computational imaging. In *2022 IEEE International Conference on Communications Workshops (ICC Workshops)*, 842–847 (IEEE, 2022).
3. Zhang, J. A. et al. Enabling joint communication and radar sensing in mobile networks-A survey. *IEEE Commun. Surv. Tutor.* **24**, 306–345 (2021).
4. Liu, F. et al. Integrated sensing and communications: Toward dual-functional wireless networks for 6G and beyond. *IEEE J. Sel. Areas Commun.* **40**, 1728–1767 (2022).
5. Wang, J., Lian, J. & Zhu, G. A weighted Mahalanobis distance target sensing strategy for underwater ISAC systems. *IEEE Wirel. Commun. Lett.* **13**(1), 79–83 (2023).
6. Zhou, W., Zhang, R., Chen, G. & Wu, W. Integrated sensing and communication waveform design: A survey. *IEEE Open J. Commun. Soc.* **3**, 1930–1949 (2022).
7. Zhong, K., Hu, J., Pan, C., Deng, M. & Fang, J. Joint waveform and beamforming design for RIS-aided ISAC systems. *IEEE Signal Process. Lett.* **30**, 165–169 (2023).
8. Li, P., Li, M., Liu, R., Liu, Q. & Swindlehurst, A. L. MIMO-OFDM ISAC waveform design for range-Doppler sidelobe suppression. *IEEE Trans. Wirel. Commun.* **24**(2), 1001–1015 (2024).
9. Zhang, J. et al. Intelligent waveform design for integrated sensing and communication. *IEEE Wirel. Commun.* https://doi.org/10.1109/MWC.003.2400044 (2024).
10. Xu, Z. & Petropulu, A. A bandwidth efficient dual-function radar communication system based on a MIMO radar using OFDM waveforms. *IEEE Trans. Signal Process.* **71**, 401–416 (2023).
11. Zhang, K. *et al.* Radar sensing via OTFS signaling: A delay Doppler signal processing perspective. In *ICC 2023 - IEEE International Conference on Communications*, 6429–6434. https://doi.org/10.1109/ICC45041.2023.10279816 (2023).
12. Liu, F. et al. Toward dual-functional radar-communication systems: Optimal waveform design. *IEEE Trans. Signal Process.* **66**, 4264–4279 (2018).
13. Liu, F., Masouros, C., Li, A., Sun, H. & Hanzo, L. MU-MIMO communications with MIMO radar: From co-existence to joint transmission. *IEEE Trans. Wirel. Commun.* **17**, 2755–2770 (2018).
14. Wang, Z., Liu, Y., Mu, X. & Ding, Z. NOMA inspired interference cancellation for integrated sensing and communication. In *ICC 2022-IEEE International Conference on Communications*, 3154–3159 (IEEE, 2022).
15. Wang, J. et al. A power-domain non-orthogonal integrated sensing and communication waveform design using OFDM. *IEEE Wirel. Commun. Lett.* **13**(4), 984–8 (2024).
16. Li, H. Dirty paper coding for waveform synthesis in integrated sensing and communications: A broadcast channel approach. In *ICC 2022-IEEE International Conference on Communications*, 1568–1573 (IEEE, 2022).
17. Li, D. *et al.* Joint precoding and jamming design for secure transmission in NOMA-ISAC networks. In *2022 14th International Conference on Wireless Communications and Signal Processing (WCSP)*, 764–769 (IEEE, 2022).
18. Wang, J., Lian, J., Zhu, G., Wang, Q. & Wang, Y. Hybrid demodulation: A optimal demodulation scheme for MU-MIMO-ISAC systems. In *2024 IEEE/CIC International Conference on Communications in China (ICCC Workshops)*, 823–828 (IEEE, 2024).
19. Xiong, Y. et al. On the fundamental tradeoff of integrated sensing and communications under Gaussian channels. *IEEE Trans. Inf. Theory* **69**(9), 5723–51 (2023).
20. He, X. & Huang, L. Joint MIMO communication and MIMO radar under different practical waveform constraints. *IEEE Trans. Veh. Technol.* **69**, 16342–16347 (2020).
21. Chen, L., Wang, Z., Du, Y., Chen, Y. & Yu, F. R. Generalized transceiver beamforming for DFRC with MIMO radar and MU-MIMO communication. *IEEE J. Sel. Areas Commun.* **40**, 1795–1808 (2022).
22. Liu, X. et al. Joint transmit beamforming for multiuser MIMO communications and MIMO radar. *IEEE Trans. Signal Process.* **68**, 3929–3944 (2020).

23. Wang, Z., Mu, X., Liu, Y. & Ding, Z. Exploiting sensing signal in ISAC: A NOMA inspired scheme. *arXiv preprint* arXiv:2201.04547 (2022).
24. Hong, Y., Thaj, T. & Viterbo, E. *Delay-Doppler Communications: Principles and Applications* (Academic Press, 2022).
25. Bazzi, A. & Chafii, M. Mutual information based pilot design for ISAC. *IEEE Trans. Commun.* **73**, 7914–7930. https://doi.org/10.1109/TCOMM.2025.3545658 (2025).
26. Bazzi, A. & Chafii, M. On integrated sensing and communication waveforms with tunable papr. *IEEE Trans. Wirel. Commun.* **22**, 7345–7360. https://doi.org/10.1109/TWC.2023.3250263 (2023).
27. Choi, J. On the power allocation for a practical multiuser superposition scheme in noma systems. *IEEE Commun. Lett.* **20**, 438–441 (2016).

Acknowledgements

This work was supported by the CETC Tianao Innovation Theory & Technology Cluster Fund, the Fund of the National Science Foundation of China (NSFC) (Program No.52571390), and the Fundamental Research Funds for the Central Universities (D5000230324), Shaanxi Provincial Science and Technology Plan (2025JC-YBQN-962), and Scientist & Engineer Team Development: Standard Project (2025JH-KGYB-0041).

Author contributions

G.L. and J.L. conceived the experiment(s). G.L, L.X. and J.D. conducted the experiment(s). Y.S., D.N., and Y.W. analysed the results. J.W., Y.G., and P.W. provided supervision and funding. All authors reviewed the manuscript.

Declarations

Competing interests

The authors declare no competing interests.

Additional information

Correspondence and requests for materials should be addressed to J.L. or P.W.